Nonlinear Dyn (2019) 97:1051–1066
https://doi.org/10.1007/s11071-019-05030-5

ORIGINAL PAPER

Hybrid modeling and predictive control of intelligent vehicle longitudinal velocity considering nonlinear tire dynamics

Xiaoqiang Sun · Houzhong Zhang · Yingfeng Cai · Shaohua Wang · Long Chen

Received: 26 July 2018 / Accepted: 27 May 2019 / Published online: 10 June 2019

Abstract A hybrid model predictive control (HMPC) strategy is proposed in this paper to autonomously regulate intelligent vehicle longitudinal velocity considering nonlinear tire dynamics. Since the tire longitudinal dynamics, which has significant influence on vehicle longitudinal velocity control performance, exhibits highly nonlinear dynamical behaviors, the piecewise affine (PWA) identification is conducted firstly based on experimental data to accurately model the tire longitudinal dynamics. On this basis, due to that the intelligent vehicle needs to be operated in two distinct modes (drive and brake) for autonomous velocity regulation and because of the affine submodel switching behaviors of the PWA-identified tire model, the intelligent vehicle longitudinal dynamics control process considered in this work can be regarded as a hybrid system with both continuous variables and discrete operating modes. Thus, the mixed logical dynamical framework is further used to model the intelligent vehicle longitudinal dynamics, and a HMPC controller, which allows us to optimize the switching sequences of the operation modes (binary control inputs) and the torques acted on the wheels (continuous control inputs), is tuned based on online mixed-integer quadratic programming. Simulation results finally demonstrate the effectiveness of the proposed HMPC controller for intelligent vehicle longitudinal velocity regulation under typical driving conditions.

Keywords Intelligent vehicle · Longitudinal dynamics · Hybrid modeling · Model predictive control · Nonlinear tire dynamics

X. Sun (✉) · H. Zhang · Y. Cai · L. Chen
Automotive Engineering Research Institute,
Jiangsu University, Jiangsu 212013, Zhenjiang,
People's Republic of China
e-mail: sunxqujs@126.com

S. Wang
School of Automotive and Traffic Engineering,
Jiangsu University, Jiangsu 212013, Zhenjiang,
People's Republic of China

List of symbols

a_x	Vehicle acceleration along the forward direction
A_w	Windward area
c	Number of the PWA submodels
C_D	Aerodynamic resistance coefficient
f_R	Rolling resistance coefficient
F_a	Vehicle accelerating resistance
F_G	Vehicle climbing resistance
F_R	Vehicle rolling resistance
F_w	Vehicle aerodynamic resistance
F_z	Tire vertical load
F_xl	Longitudinal forces generated by the left driving tire
F_xr	Longitudinal forces generated by the right driving tire
F_i	Coefficient matrices of the polyhedral region
g_i	Coefficient matrices of the polyhedral region

g	Acceleration of gravity
i_r	Road slope angle
κ	Longitudinal slip coefficient
k	Number of the data points
m_v	Vehicle curb weight
m_c	Vehicle loading weight
M_{rr}	Rolling resistance torque
n_y	PWA model orders
n_u	PWA model orders
Q_y	Positive penalty weighting parameters
Q_u	Positive penalty weighting parameters
N	Control horizon
r_d	Effective wheel rolling radius
T_s	Drive torque acted on the wheel
T_b	Brake torque acted on the wheel
T_r	Rolling resistance torque
$u(t)$	MLD system inputs
υ_w	Speed of the tire–road interface
υ_{wl}	Speed of the left tire–road interface
υ_{wr}	Speed of the right tire–road interface
υ_i	Initial vehicle velocity
υ_v	Vehicle actual velocity
$y(t)$	PWA model output
ϑ_i	Parameter vectors defining each submodel
$\varphi(t)$	Regression vector of the PWA model
χ_i	Whole polyhedral region of the affine submodels
Θ	Moment of inertia of the wheels
ρ_a	Air density
Ω_w	Wheel angular velocity

Abbreviations

MLD	Mixed logical dynamical
PWA	Piecewise affine
HMPC	Hybrid model predictive control
ITS	Intelligent transportation systems
MPC	Model predictive control
MIQP	Mixed-integer quadratic programming
MPT	Multi-parametric programming technology

1 Introduction

With the continuous growth of car ownership, traffic accidents and traffic jams have become the urgent problems to be solved in the world [1–5]. Intelligent transportation systems (ITS), which are the integrated applications of artificial intelligence, information communication, traffic planning and automatic control, have emerged as an efficient way of improving traffic capacity, reducing traffic accidents, and providing more choices for travelers [6–8]. As an important aspect of ITS, intelligent vehicles are likely to play a major role in future transportation systems, since they can provide many potential advantages, such as environment perception, autonomous decision and motion control [9–12]. Motivated by this, there have been a lot of researches conducted on intelligent vehicles, among which the longitudinal velocity control, which aims at ensuring passenger safety and comfort, has attracted the attention of several researchers [13,14].

To autonomously regulate the longitudinal velocity of an intelligent vehicle, many different types of controllers are designed based on the development of mathematical models to simulate the longitudinal dynamics responses of the intelligent vehicle. In [15], a longitudinal vehicle model was established based on the assumption that no slip occurs at the tire–road interface. Dias et al. [16] proposed a longitudinal model of an autonomous car, whose structure is conceived from the vehicle's physics equations and parameters are estimated using experimental data. Lydie et al. [17] designed a shared vehicle longitudinal controller based on the vehicle longitudinal model at low speed with no-slip assumption. In [18], a highly nonlinear model of the vehicle longitudinal motion was obtained, among which the longitudinal slip is captured through the Kiencke's tire model. Hou et al. [19] developed an accurate, but simple longitudinal vehicle model by combining theoretical analysis and vehicle test data. However, most previous researches on vehicle longitudinal control were based on simple models not accounting for the tire–road interaction. Although some studies relied on more compete models that account for the nonlinear tire dynamics, the parameters of these tire models were difficult to fit from experimental data, and some models were not simple enough to be utilizable in control design.

Modeling the tire–road interaction involves multiple aspects relevant to tire characteristics and to environmental factors, which make it a quite complex issue. Several tire models, e.g., the unified semi-empirical model [20], the magic formula model [21] and the Dugoff's model [22], have been developed with quite different properties. There is no doubt that model-based control strategies rely heavily on precise models to make accurate system predictions. Since the tire–road interaction has significant influence on vehicle longitudinal control performance, the tire model must reflect the tire longitudinal dynamics accurately. Meanwhile, as mentioned before, the most suitable tire model should also present the best accuracy/simplicity compromise for control design use. From this viewpoint, in this study, for intelligent vehicle longitudinal velocity controller design, the nonlinear tire longitudinal dynamics is considered to be approximated by the piecewise affine (PWA) model, which is also the first major contribution of this study.

The PWA systems are a special class of nonlinear systems established by partitioning the state-input domain into a limited number of polyhedral regions and obtaining the affine submodels in each region [23–25]. Since the PWA model has universal approximation capability, arbitrarily nonlinear system, which is sufficiently smooth, can be approximated well by a PWA model [26]. In addition, among different frameworks of hybrid systems, the PWA systems have been also suitably used for hybrid controller design due to their equivalencies to other classes of hybrid systems [27–29]. In [30], a direct torque control drive of three-phase induction motor was modeled by the PWA functions, and a constrained finite-time optimal control problem was set up and solved using model predictive control (MPC) method based on the derived hybrid model. Li et al. [31] proposed to model a constrained nonlinear quarter-car active suspension as a PWA system, and then, a hybrid MPC suspension controller was designed on this basis. Putz et al. [32] obtained a PWA model for flotation plant by applying identification techniques for different operating conditions, and a hybrid MPC methodology was developed based on the system PWA model.

Note that to cover the whole range of operation, the affine submodels of the PWA system should switch between different operating conditions, and for autonomous velocity regulation, the intelligent vehicle needs to be operated in two distinct modes (drive and brake). Thus, in this paper, the intelligent vehicle longitudinal dynamics with nonlinear tire model presented by the PWA form is regarded as a typical hybrid dynamical system. Such a class of hybrid systems can be further described as MLD systems, which are well suited for the formulation of MPC problems for hybrid systems [33,34]. The derived MLD model is used to predict the future behaviors of the hybrid system, and on this basis, a hybrid MPC (HMPC) approach can be adopted to develop the intelligent vehicle longitudinal velocity controller, which is the other major contribution of this study. It is formally proved through simulations that the developed HMPC controller can optimize the switching sequences of the operation modes and the torques acted on the wheels simultaneously with a more accurate tire model.

The originality of this paper is that the PWA model of the tire nonlinear dynamics is identified through the experimental data, and a HMPC controller is tuned to control the intelligent vehicle longitudinal velocity based on the system MLD model. That is, the study includes two major innovations. The first is the identification of the PWA model of the tire longitudinal dynamics, which not only provides a novel modeling approach for the tire dynamics, but also presents the best model accuracy/simplicity compromise for the longitudinal velocity control design. The other contribution is the design of the system HMPC controller, which allows us to optimize the switching sequences of the operation modes and the torques acted on the wheels simultaneously during the intelligent vehicle longitudinal velocity control process.

The paper is organized as follows. Section 2 is devoted to identifying the tire longitudinal dynamics as a PWA system based on experimental data. In Sect. 3, the intelligent vehicle longitudinal dynamics with the PWA tire model is modeled as a hybrid system based on the MLD framework. The obtained hybrid model is used in Sect. 4 to design a HMPC controller for intelligent vehicle longitudinal velocity regulation. Simulation results for all considered cases are given and analyzed in Sect. 5 to illustrate the controller performances. Section 6 concludes the paper with a summary and an outlook.

2 PWA modeling of tire longitudinal dynamics

Tire model is used to reflect the input–output characteristics of the tire under specific driving conditions, which are shown in Fig. 1 [35]. For different research emphases, the tire model can be further classified into three categories, among which the tire longitudinal dynamics has significant influence on the vehicle driving stability and braking safety. In addition, the relationships between the longitudinal force generated by the tire and its influencing factors are entirely differ-

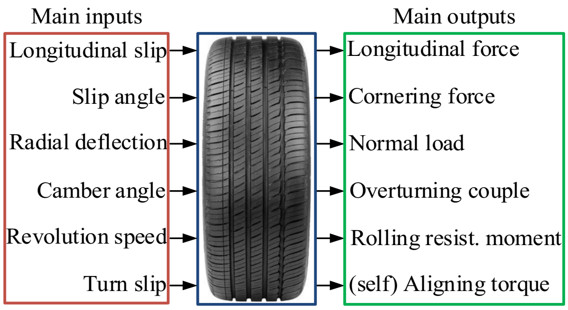

Fig. 1 Input–output characteristics of the tire

Fig. 2 Experimental setup of the tire longitudinal dynamics

ent for different driving conditions, thus it is of great significance to establish an accurate tire model. One of the main contributions of this paper is just to establish the tire longitudinal dynamics model through the PWA identification method based on the driven data.

3 Tire longitudinal dynamics tests

To obtain the accurate test data about the tire longitudinal dynamics, the tire tests are conducted using a flat-plate tire test bench. The experimental setup of the tire longitudinal dynamics is shown in Fig. 2. During the test procedure, the tire pressure is assumed to be constant, and the tire slip angle is assumed to be zero. These assumptions are also the research premises of this paper. The parameter settings of the tire tests are given in Table 1, among which the two different longitudinal adhesion coefficients are estimated according to the materials of the rolling plates.

Table 1 List of parameter settings

Parameter	Setting
Tire pressure (kPa)	880
Vertical load (N)	3124, 6530, 8036, 9468, 11760
Slip angle (rad)	0
Longitudinal slip	$-1 \sim 0.5$
Adhesion coefficient	0.34 (low) 0.77 (high)

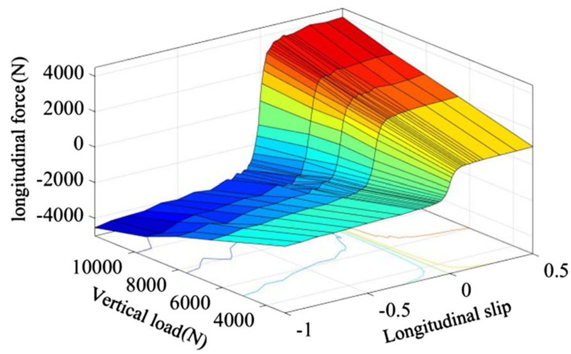

Fig. 3 Tire test results for low adhesion coefficient

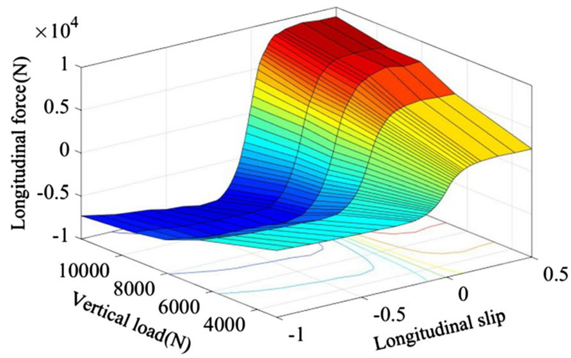

Fig. 4 Tire test results for high adhesion coefficient

The tire longitudinal dynamics test results for the two different longitudinal adhesion coefficients are shown in Figs. 3 and 4, respectively. As it can be observed from the tests results, the relationship between the tire longitudinal force and its influence factors is manifested as an irregular curved surface. If these curved surfaces can be decomposed into several flat surfaces for different operating regions, the nonlinear tire longitudinal dynamics can then be linearized accurately. This idea is just the research object of the PWA identification of the tire longitudinal dynamics.

By further comparing the tire longitudinal dynamics test results for the two longitudinal adhesion coefficients, it can be found that the relationship between the tire longitudinal force and the road longitudinal adhesion coefficient is linear approximately for the same operating region. Therefore, in this paper, the road adhesion coefficient is not considered as an impact factor of the tire longitudinal dynamics. This simplification is not only consistent with the actual situation, but also reduces the complexity of the PWA identification. In addition, several research works have been devoted to estimate the road longitudinal adhesion coefficient [36]; thus, this factor can be regarded as a known condition for the tire longitudinal dynamics modeling.

4 PWA identification

A PWA model of the dynamical system is defined as [37]:

$$y(t) = \begin{cases} \vartheta_1^T \begin{bmatrix} \varphi(t) \\ 1 \end{bmatrix} + \varepsilon(t), & if\ \varphi(t) \in \chi_1 \\ \vdots \\ \vartheta_c^T \begin{bmatrix} \varphi(t) \\ 1 \end{bmatrix} + \varepsilon(t), & if\ \varphi(t) \in \chi_c \end{cases} \tag{1}$$

where $y(t)$ is the PWA model output, $\vartheta_i (i = 1, \ldots, c)$ are the parameter vectors defining each submodel, c is the number of the submodels, $\varphi(t)$ represents the regression vector. The regression vector $\varphi(t)$ studied in this paper, which consists of the system past inputs and outputs, is formed as:

$$\begin{aligned}\varphi(t) = [&y(t-1), \ldots, y(t-n_y), \\ &u(t-1), \ldots, u(t-n_u)]^T\end{aligned} \tag{2}$$

where n_y and n_u are the PWA model orders, $u(t)$ is the input to the system. $\chi_i (i = 1, \ldots, c)$ represents the whole polyhedral region of the affine submodels, and each region χ_i is a convex polyhedron represented in the following form:

$$\chi_i = \{F_i \varphi(t) + g_i \le 0\} \tag{3}$$

where F_i and g_i are the corresponding coefficient matrices. By letting $M_i = [F_i g_i]$, $(i = 1, \ldots, c)$, the convex polyhedron region χ_i can be rewritten as:

$$\chi_i = \left\{M_i\ [\varphi(t)\ 1]^T \le 0\right\} \tag{4}$$

The PWA system defined by the above equations can be regarded as a collection of affine subsystems connected by dynamical switches which depend on the partition of the polyhedral region. The PWA identification problem solved in this paper is just to obtain a PWA model for the tire longitudinal dynamics based on the experimental data. It mainly includes the following two steps:

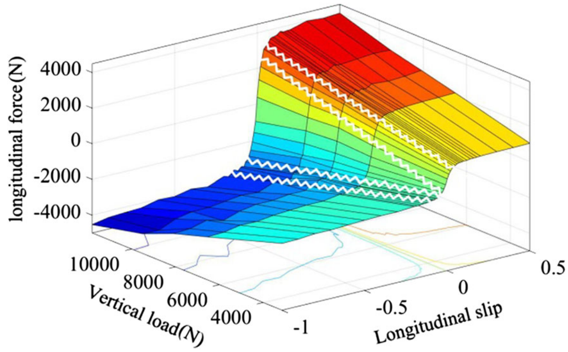

Fig. 5 All five affine submodels of the system derived coarsely from steady-state response

4.1 Segmentation

At the first step, the number of the affine submodels and the coefficient matrices of hyperplanes are determined. To find a good balance between the number of the submodels and the overall fitting accuracy, several approaches for region partitioning have been proposed [38]. Considering the PWA identification problem researched in this study, heuristic approach is used according to the system steady-state response surfaces. By further observing the surface shape shown in the figure, it can be concluded that five affine submodels can reasonably approximate these curved surfaces, which determines the number of the affine submodels as five. Figure 5 shows all five affine submodels of the system derived coarsely from steady-state responses. In this paper, to distinguish between these affine submodels and derive the space line equations for the nonlinear relationship shown in Fig. 3, the following operating points are listed as:

$$\begin{cases} A(-0.19, 11800, -3450); \\ B(-0.04, 11800, -2505); \\ C(0.03, 11800, 2815); \\ D(0.07, 11800, 3400); \end{cases} \quad \begin{cases} E(0.036, 3124, 799.6); \\ F(-0.02, 3124, -425.2); \\ G(-0.03, 3468, -607.6); \\ L(-0.03, 3124, -529.2); \\ I(-0.07, 3124, -805.6); \end{cases}$$

Projecting these nine data points on the xy plane results in H_i coefficients, which are described as the following five linear equations:

$$\begin{cases} F_z = -69636\kappa - 1751.7; \\ F_z = -867600\kappa - 22904; \\ F_z = -34797\kappa + 2410.5; \\ F_z = 137960\kappa + 7662.2; \\ F_z = 260520\kappa - 6441.4; \end{cases} \tag{5}$$

where F_z is the tire vertical load, κ is the longitudinal slip coefficient. These five linear equations define the partition of the operating region.

4.2 Regression

After repeated analyses and comparisons, the order of the affine submodels is finally determined as: $n_y = 2$ and $n_u = 1$. Once the operating region is partitioned and the order of the submodels is determined, the parameter vectors of the affine submodels can then be estimated by using the least-square algorithm. On the basis of the aforementioned segmentation, the data points have been classified into several clusters; thus, the regression aim is to estimate an affine model for each cluster. If N data points are provided for a fixed number of the affine submodels, the considered regression problem can be formulated as follows [39]:

$$\begin{aligned} &\lambda_{ki} = \begin{cases} 1 \text{ if } \varphi(k) \in \chi_i \\ 0 \text{ otherwise} \end{cases} \quad k = 1, \ldots, N,\ i = 1, \ldots, c \\ &\min_{\vartheta_i} \frac{1}{N} \sum_{k=1}^{N} \sum_{i=1}^{c} \left(y_k - \vartheta_i^T \begin{bmatrix} \varphi(t) \\ 1 \end{bmatrix} \right)^2 \lambda_{ki} \end{aligned} \tag{6}$$

Solving the problem shown in Eq. (6) for $\vartheta_i c$ will result in five affine submodels with parameters as follows:

$$\begin{cases} F_x(k) = -0.156F_x(k-1) + 0.183F_x(k-2) \\ \qquad +461.72\kappa(k-1) - 0.312F_z(k-1) + 202.44 \\ if\ F_z \le -69636\kappa - 1751.7 \end{cases}$$

$$\begin{cases} F_x(k) = -0.284F_x(k-1) + 0.267F_x(k-2) \\ \qquad +6910\kappa(k-1) - 0.22F_z(k-1) + 364.65 \\ if\ F_z > -69636\kappa - 1751.7\& \\ (F_z \le -867600\kappa - 22904 | F_z \le -34797\kappa + 2410.5) \end{cases}$$

$$\begin{cases} F_x(k) = 1.304F_x(k-1) - 1.218F_x(k-2) \\ \qquad +71757.1\kappa(k-1) - 0.145F_z(k-1) + 2076.57 \\ if\ F_z > \text{-}867600\kappa - 22904\& F_z \ge 137960\kappa + 7662.2 \end{cases}$$

$$\begin{cases} F_x(k) = -0.424F_x(k-1) + 0.367F_x(k-2) \\ \qquad +22050\kappa(k-1) + 0.215F_z(k-1) - 684.12 \\ if\ F_z < 137960\kappa + 7662.2\& F_z > \text{-}34797\kappa + 2410.5 \\ \& F_z \ge 260520\kappa - 6441.4 \end{cases}$$

$$\begin{cases} F_x(k) = -0.168F_x(k-1) + 0.157F_x(k-2) \\ \qquad +505\kappa(k-1) + 0.298F_z(k-1) - 151.42 \\ if\ F_z < 260520\kappa - 6441.4 \end{cases}$$

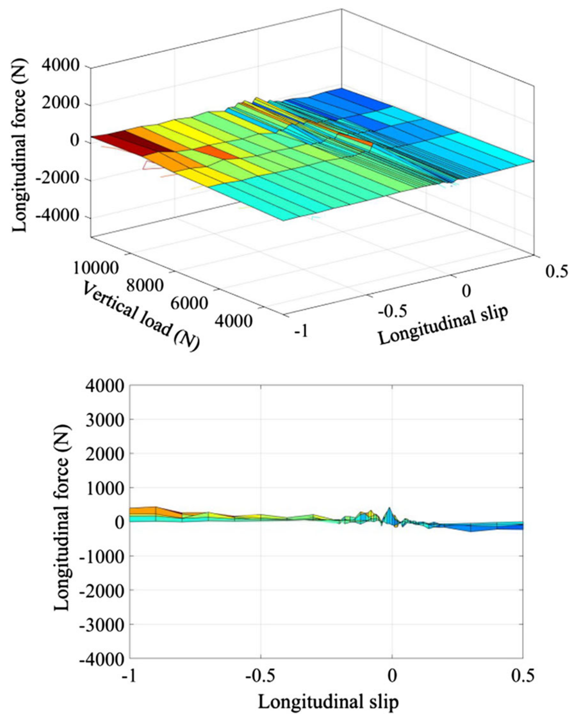

Fig. 6 Fitting error between the PWA model output and the experimental data for low adhesion coefficient

4.3 Accuracy validation

To validate the accuracy of the identified PWA model, its simulation results are compared with the experimental data. The fitting error, i.e., the tire longitudinal force difference between the PWA model output and the experimental data for low adhesion coefficient, is shown in Fig. 6. It can be concluded that the error distribution is concentrated near zero, and its amplitude range is relatively small compared with that of the actual tire longitudinal force, which indicates that the PWA model can effectively approximate the dynamical behaviors of the tire longitudinal dynamics.

Since the tire longitudinal dynamics with different road adhesion coefficients are assumed to be linearly dependent in this study, thus on the basis of the identified PWA model for low adhesion coefficient, the fitting error between the PWA model and the experimental data for high adhesion coefficient can be further obtained as Fig. 7. As it can be demonstrated from the figure, similar conclusion can be obtained as the previous scenario, i.e., the output of the PWA model matches the experimental results accurately, which fur-

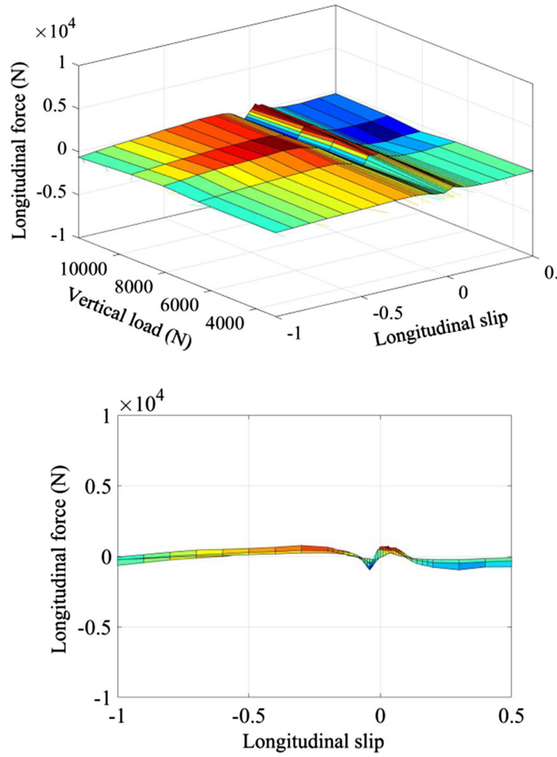

Fig. 7 Fitting error between the PWA model output and the experimental data for high adhesion coefficient

ther validates the effectiveness of the PWA identification method.

5 System hybrid modeling

Hybrid dynamic model is used to describe a class of systems which involve both continuous and discrete dynamics. Since the intelligent vehicle longitudinal dynamics with the PWA tire model has typical hybrid characteristics, the system hybrid modeling is conducted in this section for the following HMPC controller design.

6 Vehicle longitudinal dynamics

As shown in many previous works, the vehicle longitudinal dynamics model can be established based on Newtonian mechanics. Thus, the total vehicle driving resistance which also represents the vehicle driving force demands (F_{Dem}) can be obtained as follows [40–43]:

$$F_{\mathrm{Dem}} = F_{\mathrm{a}} + F_{\mathrm{G}} + F_{\mathrm{R}} + F_{\mathrm{w}} \tag{7}$$

where F_{a} represents the vehicle accelerating resistance, F_{G} represents the vehicle climbing resistance, F_{R} represents the rolling resistance, F_{w} represents the aerodynamic resistance. All these resistances can be approximatively given by [44]:

$$\begin{cases} F_{\mathrm{a}} = (m_{\mathrm{v}} + m_{\mathrm{c}} + \Theta/r_d^2)a_x \\ F_{\mathrm{G}} = (m_{\mathrm{v}} + m_{\mathrm{c}})gi_r \\ F_{\mathrm{R}} = f_{\mathrm{R}}(m_{\mathrm{v}} + m_{\mathrm{c}})g \\ F_{\mathrm{w}} = C_{\mathrm{D}}A_{\mathrm{w}}\frac{\rho_{\mathrm{a}}}{2}v_v^2 \end{cases} \tag{8}$$

where m_{v} and m_{c} are the vehicle curb weight and the vehicle loading weight, respectively, Θ is the moment of inertia of the wheels, r_{d} is the effective wheel rolling radius, a_{x} is the vehicle acceleration along the forward direction, g is the acceleration of gravity, i_{r} is the road slope angle which uses radian as unit, f_{R} is the rolling resistance coefficient, C_{D} is the aerodynamic resistance coefficient, A_{w} is the windward area, v_{v} is the vehicle velocity, ρ_{a} is the air density.

Except for the aerodynamic resistance, all external efforts acting on the vehicle are generated at the wheel–road contact. Therefore, the accurate modeling of the tire longitudinal dynamics is essential for controlling the intelligent vehicle. For those tire models established on the assumption that no slip occurs at the tire–road interface, the longitudinal force generated by the tire (F_{x}) is described by:

$$F_{\mathrm{x}} = \frac{T_{\mathrm{s}} - T_{\mathrm{b}} - M_{\mathrm{rr}}}{r_{\mathrm{d}}} \tag{9}$$

where T_{s} represents the drive torque acted on the wheel, T_{b} represents the brake torque acted on the wheel, M_{rr} denotes the rolling resistance torque. The tire longitudinal dynamics model shown in Eq. (9) may be sufficient for the longitudinal control design when driving on the dry asphalt road, but for the icy and slippery roads, the tire longitudinal dynamics will have behavioral changes and variations due to slip occurrence. Therefore, the tire longitudinal force described by Eq. (9) is no longer accurate sufficiently for these driving conditions. To solve this problem, the tire longitudinal dynamics is identified through the PWA approach in this paper. Based on the identification results, a schematic representation of the PWA tire model is shown in Fig. 8.

Invoking the dynamic fundamental principle, the wheel dynamics can be described by the following equation:

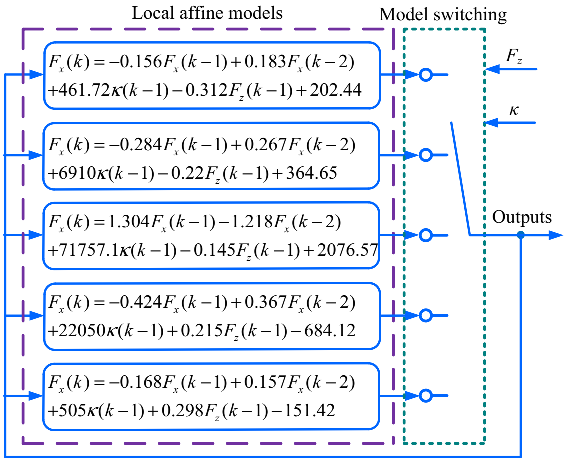

Fig. 8 Schematic representation of the PWA tire model

$$\Theta \frac{\mathrm{d}\Omega_w}{\mathrm{d}t} = T_\mathrm{s} - T_\mathrm{b} - F_\mathrm{x} r_\mathrm{d} - T_\mathrm{r} \tag{10}$$

where Ω_w denotes the wheel angular velocity, T_r denotes the rolling resistance torque. Based on the relation $v_\mathrm{w} = r_\mathrm{d}\Omega_\mathrm{w}$, the following equation can be obtained as:

$$\dot{v}_\mathrm{w} = \frac{T_\mathrm{s} - T_\mathrm{b} - F_\mathrm{x} r_\mathrm{d} - T_\mathrm{r}}{\Theta} r_\mathrm{d} \tag{11}$$

where v_w represents the speed of the tire–road interface. On this basis, the tire longitudinal slip is defined as follows:

$$\begin{cases} \kappa = 1 - \frac{v_\mathrm{v}}{v_\mathrm{w}} = 1 - \frac{v_\mathrm{v}}{r_\mathrm{d}\Omega_\mathrm{w}} & \text{in acceleration mode} \\ \kappa = \frac{v_\mathrm{v}}{v_\mathrm{w}} - 1 = \frac{v_\mathrm{v}}{r_\mathrm{d}\Omega_\mathrm{w}} - 1 & \text{in deceleration mode} \end{cases} \tag{12}$$

According to Eqs. (7) and (8), the vehicle velocity v_v, i.e., the linear velocity of the wheel center, can be obtained as:

$$\dot{v}_\mathrm{v} = \frac{F_\mathrm{x} - F_\mathrm{G} - F_\mathrm{R} - F_\mathrm{w}}{m_\mathrm{v} + m_\mathrm{c} + \Theta/r_d^2} \tag{13}$$

The above equations together with the identified PWA tire model describe the vehicle longitudinal dynamics. To make clear the research object in this paper, the intelligent vehicle longitudinal dynamics model is developed based on a front-wheel-drive vehicle. Thus, the global diagram of the vehicle longitudinal dynamics is further illustrated by Fig. 9.

In the figure, F_xl and F_xr represent the longitudinal forces generated by the left driving tire and the right driving tire, respectively, v_wl and v_wr represent the speeds of the left tire–road interface and the right tire–road interface, v_i is the initial vehicle velocity.

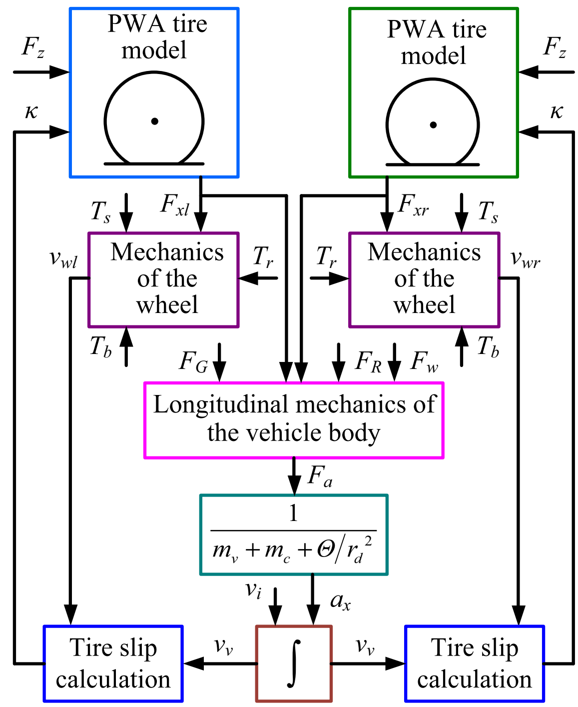

Fig. 9 Global diagram of the vehicle longitudinal dynamics

7 Dynamic hybrid model

To cover the whole operation range of the intelligent vehicle longitudinal dynamics which involves both discrete and continuous variables, the system hybrid model is considered to be established in this section. Considering the following formulation of the system hybrid MPC strategy and the equivalent between the PWA model and the MLD model, the intelligent vehicle longitudinal dynamics with the PWA-identified tire model is formulated by the MLD systems, which can be generalized by [45,46]:

$$\begin{cases} x(t+1) = Ax(t) + B_1 u(t) + B_2\delta(t) + B_3 z(t), \\ y(\mathrm{t}) = Cx(\mathrm{t}) + D_1 u(\mathrm{t}) + D_2\delta(\mathrm{t}) + D_3 z(\mathrm{t}), \\ E_2\delta(\mathrm{t}) + E_3 z(\mathrm{t}) \le E_1 u(\mathrm{t}) + E_4 x(\mathrm{t}) + E_5, \end{cases} \tag{14}$$

where $x \in \Re^{n_\mathrm{r}} \times \{0,1\}^{n_\mathrm{b}}$, $u \in \Re^{m_\mathrm{r}} \times \{0,1\}^{m_\mathrm{b}}$, $y \in \Re^{p_\mathrm{r}} \times \{0,1\}^{p_\mathrm{b}}$ denote the system state, input and output vectors, respectively. It is noted that these vectors can include both continuous and discrete variables. In addition, $\delta \in \{0,1\}^{r_\mathrm{b}}$ and $z \in \Re^{r_\mathrm{r}}$ denote the auxiliary binary and continuous variables, respectively, which are defined for the convenience of the system hybrid modeling. The evolution of the system state variables is described by the state matrix A and the input

Table 2 HYSDEL list of hybrid systems

SYSTEM sample {
INTERFACE {
STATE { REAL cs_1, cs_2, $\cdots$, cs_{nr}; BOOL δs_1, δs_2, $\cdots$, δs_{nb}; }
INPUT { REAL ci_1, ci_2, $\cdots$, ci_{mr}; BOOL δi_1, δi_2, $\cdots$, δi_{mb};}
OUTPUT { REAL co_1, co_2, $\cdots$, co_{pr}; BOOL δo_1, δo_2, $\cdots$, δo_{pb};}
PARAMETER { REAL v_1= ; v_2= ; $\cdots$, v_n= ;}}
IMEPLEMENTATION {
AUX { REAL ca_1, ca_2, $\cdots$, ca_{rr}; BOOL δa_1, δa_2, $\cdots$, δs_{rb};}
CONTINUOUS {continuous state update equations}
AUTOMATA {binary state transition equations}
LINEAR {linear relations between continuous variables}
LOGIC {logical relations between binary variables}
AD {define binary variables from continuous variables}
DA {define continuous variables from binary variables}
MUST {specifies input/state/output constraints}
OUTPUT {static linear and logic relations for output}}}

matrices B_1, B_2 and B_3. Similarly, the output matrix C and the matrices D_1, D_2 and D_3 describe the evolution of the system output. The matrices E_1 to E_5 define the system inequalities, which are incorporated when logic rules are transformed into mixed-integer inequalities. The MLD models have successfully proved to be able to recast hybrid system control problem into mixed-integer linear or quadratic programming problem solvable via efficient solvers [47]. This feature has led to this model to be widely used in the formulation of the hybrid system MPC strategies.

Since the traditional modeling procedures for the MLD systems are inefficient and tedious, a novel language called HYSDEL available for MATLAB is developed by researchers [48]. The HYSDEL fully automates the process of generating the matrices associated with a MLD model defined by Eq. (14). Table 2 shows the HYSDEL structure used to establish a MLD model suitable to be used in the HMPC strategy.

Based on the aforementioned HYSDEL structure, how the intelligent vehicle longitudinal dynamics with the PWA tire model can be formulated as a MLD system is introduced in the following sections. The vehicle longitudinal dynamics is characterized firstly by two state variables, i.e., the vehicle (chassis) speed v_{v} and the speed of the tire–road interface v_{w}. To achieve the autonomous velocity regulation, the system input variables are defined as:

$$u = [\delta_{\mathrm{s}}\ \delta_{\mathrm{b}}\ T_{\mathrm{s}}\ T_{\mathrm{b}}]^T \tag{15}$$

where δ_{s} and δ_{b} are binary control variables which have the following correspondence with the system operation modes:

$$\begin{cases} [\delta_{\mathrm{s}} = 1] \leftrightarrow \ \text{drive mode is work} \\ [\delta_{\mathrm{b}} = 1] \leftrightarrow \ \text{brake mode is work} \end{cases} \tag{16}$$

Since the MLD model only allows specifying the evolution of continuous variables through linear dynamic equations, the square of velocity in the expression of the air resistance needs to be piecewise linearized. According to the vehicle velocity range, the piecewise-linear approximation of the square of velocity is given by the following equations:

$$v_{\mathrm{v}}^2 = \begin{cases} 10v_{\mathrm{v}} \quad [0 \le v_{\mathrm{v}} < 10]; \\ 30v_{\mathrm{v}} - 200 \quad [10 \le v_{\mathrm{v}} < 20]; \\ 50v_{\mathrm{v}} - 600 \quad [20 \le v_{\mathrm{v}} < 30]; \\ 70v_{\mathrm{v}} - 1200 \quad [30 \le v_{\mathrm{v}} \le 40]. \end{cases} \tag{17}$$

Based on the above approximation process, the following auxiliary variables are further defined as:

$$\begin{aligned} &[\delta_{sv1} = 1] \leftrightarrow 0 \le v_v < 10,\ [\delta_{sv2} = 1] \leftrightarrow 10 \le v_v < 20, \\ &[\delta_{sv3} = 1] \leftrightarrow 20 \le v_v < 30,\ [\delta_{sv4} = 1] \leftrightarrow 30 \le v_v < 40, \end{aligned} \tag{18}$$

where δ_{sv1} to δ_{sv4} are the defined auxiliary variables. On this basis, four continuous auxiliary variables c_{sv1} to c_{sv4} can be further defined as:

$$\begin{cases} c_{sv1} = \{\text{IF } \delta_{sv1} \text{ THEN } 10v_{\mathrm{v}} \text{ ELSE } 0\}, \\ c_{sv2} = \{\text{IF } \delta_{sv2} \text{ THEN } 30v_{\mathrm{v}} - 200 \text{ ELSE } 0\}, \\ c_{sv3} = \{\text{IF } \delta_{sv3} \text{ THEN } 50v_{\mathrm{v}} - 200 \text{ ELSE } 0\}, \\ c_{sv4} = \{\text{IF } \delta_{sv4} \text{ THEN } 70v_{\mathrm{v}} - 1200 \text{ ELSE } 0\}, \end{cases} \tag{19}$$

Therefore, the vehicle aerodynamic resistance in Eq. (9) can be rewritten by:

$$F_{\mathrm{w}} = C_{\mathrm{D}} A \frac{\rho_{\mathrm{a}}}{2} c_{\mathrm{sv}} \tag{20}$$

where $c_{sv} = c_{sv1} + c_{sv2} + c_{sv3} + c_{sv4}$.

To calculate the tire longitudinal force according to the PWA-identified model, the following five binary auxiliary variables δ_{tl1} to δ_{tl5} are firstly defined as:

$$\begin{aligned} &[\delta_{tl1} = 1] \leftrightarrow F_{\mathrm{z}} \le -69636\kappa - 1751.7, \\ &[\delta_{tl2} = 1] \leftrightarrow (F_{\mathrm{z}} > -69636\kappa - 1751.7) \\ &\quad \wedge((F_{\mathrm{z}} \le -867600\kappa - 22904) \\ &\quad \vee(F_{\mathrm{z}} \le -34797\kappa + 2410.5)) \\ &[\delta_{tl3} = 1] \leftrightarrow F_{\mathrm{z}} > -867600\kappa - 22904 \\ &\quad \wedge F_{\mathrm{z}} \ge 137960\kappa + 7662.2 \end{aligned}$$

$$
\begin{aligned}
&[\delta_{tl4}=1] \leftrightarrow F_z < 137960\kappa + 7662.2\\
&\quad \wedge F_z > -34797\kappa + 2410.5\\
&\quad \wedge F_z \geq 260520\kappa - 6441.4\\
&[\delta_{tl5}=1] \leftrightarrow F_z < 260520\kappa - 6441.4
\end{aligned} \tag{21}
$$

Then, the following five continuous auxiliary variables c_{tl1} to c_{tl5} can be defined accordingly as:

$$
\begin{cases}
c_{tl1} = \{\text{IF } \delta_{tl1} \text{ THEN } -0.156F_x(k-1)+0.183F_x(k-2)\\
\qquad +461.72\kappa(k-1)-0.312F_z(k-1)+202.44 \text{ ELSE } 0\},\\
c_{tl2} = \{\text{IF } \delta_{tl2} \text{ THEN } -0.284F_x(k-1)+0.267F_x(k-2)\\
\qquad +6910\kappa(k-1)-0.22F_z(k-1)+364.65 \text{ ELSE } 0\},\\
c_{tl3} = \{\text{IF } \delta_{tl3} \text{ THEN } 1.304F_x(k-1)-1.218F_x(k-2)\\
\qquad +71757.1\kappa(k-1)-0.145F_z(k-1)+2076.57 \text{ ELSE } 0\},\\
c_{tl4} = \{\text{IF } \delta_{tl4} \text{ THEN } -0.424F_x(k-1)+0.367F_x(k-2)\\
\qquad +22050\kappa(k-1)+0.215F_z(k-1)-684.12 \text{ ELSE } 0\},\\
c_{tl5} = \{\text{IF } \delta_{tl5} \text{ THEN } -0.168F_x(k-1)+0.157F_x(k-2)\\
\qquad +505\kappa(k-1)+0.298F_z(k-1)-151.42 \text{ ELSE } 0\},
\end{cases} \tag{22}
$$

On this basis, the longitudinal force generated by the tire can be rewritten by:

$$
F_{\mathrm{x}} = c_{tl1} + c_{tl2} + c_{tl3} + c_{tl4} + c_{tl5} \tag{23}
$$

Since the MLD model is established based on discrete-time, the derivatives of the state variables are given by:

$$
\begin{cases}
\dot{v}_{\mathrm{v}} = (v_{\mathrm{v}}(t+1) - v_{\mathrm{v}}(t))/T_{\mathrm{k}}\\
\dot{v}_{\mathrm{w}} = (v_{\mathrm{w}}(t+1) - v_{\mathrm{w}}(t))/T_{\mathrm{k}}
\end{cases} \tag{24}
$$

where T_k is the sample time. Thus, according to the above equations, the update equations for the system state variables can be obtained as:

$$
\begin{cases}
v_{\mathrm{v}}(t+1) = v_{\mathrm{v}}(t) + \frac{T_{\mathrm{k}}(F_{\mathrm{xl}}+F_{\mathrm{xr}})}{M} - \frac{T_{\mathrm{k}}(m_{\mathrm{v}}+m_{\mathrm{c}})gi_{\mathrm{r}}}{M}\\
-\frac{T_{\mathrm{k}} f_{\mathrm{R}}(m_{\mathrm{v}}+m_{\mathrm{c}})g}{M} - \frac{T_{\mathrm{k}} C_{\mathrm{D}} A \rho_{\mathrm{a}} c_{\mathrm{sv}}}{2M}\\
v_{\mathrm{w}}(t+1) = v_{\mathrm{w}}(t) + \frac{T_{\mathrm{k}}(T_{\mathrm{s}}-T_{\mathrm{b}})r_{\mathrm{d}}}{\Theta}\\
-\frac{T_{\mathrm{k}}(F_{\mathrm{xl}}+F_{\mathrm{xr}})r_{\mathrm{d}}^2}{\Theta} - \frac{T_{\mathrm{k}} T_{\mathrm{r}} r_{\mathrm{d}}}{\Theta}
\end{cases} \tag{25}
$$

where $M = m_{\mathrm{v}} + m_{\mathrm{c}} + \Theta/r_{\mathrm{d}}^2$. Since the definition of the tire longitudinal slip coefficient depends on the current driving mode (acceleration or deceleration), the tire slip coefficient can be further defined as:

$$
\kappa = \left(1 - \frac{v_{\mathrm{v}}}{v_{\mathrm{w}}}\right)\delta_{\mathrm{s}} + \left(\frac{v_{\mathrm{v}}}{v_{\mathrm{w}}} - 1\right)\delta_{\mathrm{b}} \tag{26}
$$

After defining the above system variables and determining their relationships and update equations, the MLD model of the intelligent vehicle longitudinal dynamics with the PWA-identified tire model can then be obtained directly by using the HYSDEL, which can generate the system MLD model as an encapsulation module called "HYSDEL model" in MATLAB/Simulink. The resulting MLD model mainly consists of four inputs and one output. The dimensions of all matrices shown in Eq. (14) are $A_{(2\times2)}$, $B_{1(2\times4)}$, $B_{2(2\times14)}$, $B_{3(2\times16)}$, $C_{(1\times2)}$, $D_{1(1\times4)}$, $D_{2(1\times14)}$, $D_{3(1\times16)}$, $E_{1(18\times14)}$, $E_{2(18\times16)}$, $E_{3(18\times4)}$, $E_{4(18\times2)}$, $E_{5(18\times1)}$. All system constraints are summarized in the 78 mixed-integer inequalities, which are omitted here for lack of space.

8 Hybrid controller design

The intelligent vehicle longitudinal velocity regulation system presented in this study can operate in two different modes. Meanwhile, the PWA-identified tire model needs to switch between different affine submodels to cover the whole range of operation. The switching between these operating modes and submodels would indicate a system model with a time-varying structure. Furthermore, the relationship between the longitudinal velocity and the input torques is intrinsically nonlinear. Therefore, the methodology which can tackle the switching and nonlinearity issues is worthy to be researched.

In this section, how the HMPC can deal with both discrete and continuous dynamics of the intelligent vehicle velocity regulation system is introduced. The HMPC uses the MLD model to predict the future evolution of the system within a fixed prediction horizon; thus, a finite horizon optimal control problem at each sampling instant can then be solved. On this basis, a sequence of the future control inputs is determined through the optimization procedure, which aims to minimize a given objective function and enforces fulfillment of the constraints. Then, by only applying the first control input in this sequence and by recomputing the control sequence at the next sampling time, a receding horizon policy is achieved, which provides a feedback mechanism for reference tracking.

The HMPC control aim in this study is to minimize the error between a reference and the actual vehicle longitudinal velocity, and to avoid the frequent variations in manipulated variables. By describing the optimal control of the intelligent vehicle longitudinal dynamics as a HMPC control problem, the output of the controller at each sampling instant is the solution to the following optimization problem:

$$\text{minimize} \sum_{h=0}^{N-1} \|y(h|t) - y_{\text{ref}}\|_{Q_y}^2 + \sum_{h=0}^{N-1} \|\Delta u(h|t)\|_{Q_u}^2 \tag{27a}$$

$$\begin{aligned} \text{subj.to. } & x(0|t) = x(t) \\ & x(t+1) = Ax(t) + B_1 u(t) + B_2 \delta(t) + B_3 z(t) \\ & y(\text{t}) = Cx(\text{t}) + D_1 u(\text{t}) + D_2 \delta(\text{t}) + D_3 z(\text{t}) \\ & E_2 \delta(\text{t}) + E_3 z(\text{t}) \le E_1 u(\text{t}) + E_4 x(\text{t}) + E_5 \\ & u_{\min} \le u(h|\text{t}) \le u_{\max} \\ & x_{\min} \le \Delta x(h|\text{t}) \le x_{\max} \end{aligned} \tag{27b}$$

where Q_y and Q_u are the suitable positive penalty weighting parameters, N is the control horizon, $\Delta u(h|t)$ and $\Delta x(h|t)$ are defined as:

$$\begin{cases} \Delta u(h|t) = [\delta_{\text{d}}(h|t) \\ \quad -\delta_{\text{d}}(h|t-1) \;\; \delta_{\text{b}}(h|t) - \delta_{\text{b}}(h|t-1)]^T \\ \Delta x(h|t) = [v(h|t) - v(h|t-1)] \end{cases} \tag{28}$$

Just as mentioned before, to achieve the control objectives, each term in this optimization statement has clear physical meaning in terms of the functionality of the HMPC control system for the intelligent vehicle longitudinal dynamics. The first term in the objective function represents the intelligent vehicle velocity tracking objective. Thus, error between the actual vehicle velocity and the desired value is penalized through a weighted norm, which ensures that the output of the optimal controller can help track the vehicle's desired velocity. $\Delta u(h|t)$ corresponds to the changes in the first two inputs between the two adjacent sampling instants, which is used to avoid the frequent switching of the operation modes.

By setting the following vectors:

$$\begin{cases} \Omega = \left[u^T(0|t) \;\; \cdots \;\; u^T(N-1|t)\right]^T \\ \Xi = \left[\delta^T(0|t) \;\; \cdots \;\; \delta^T(N-1|t)\right]^T \\ \Gamma = \left[z^T(0|t) \;\; \cdots \;\; z^T(N-1|t)\right]^T \end{cases} \tag{29}$$

and the general vector:

$$\Lambda = \left[\Omega^T \;\; \Xi^T \;\; \Gamma^T\right]^T \tag{30}$$

the HMPC control problem of the intelligent vehicle longitudinal dynamics with the PWA tire model can then be formulated as a mixed-integer quadratic programming (MIQP) problem, which is solved as follows [49–51]:

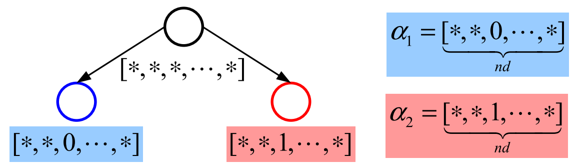

Fig. 10 Generation from parent node to sub-node

$$\begin{aligned} & \min_{\{\Lambda\}} \;\; \tfrac{1}{2}\Lambda^T S_1 \Lambda + S_2 \Lambda \\ & \text{Subj.to. } S_3 \Lambda \le S_4 \end{aligned} \tag{31}$$

where S_1, S_2, S_3 and S_4 are matrices with suitable dimensions. Considering the characteristics of the research problem in this study, the Branch and Bound method is used to solve the MIQP problem. The main idea of the Branch and Bound method for solving the MIQP problem is to lift partial or whole integer restrictions in the decision variables; thus, a series of quadratic programming (QP) problems which follow the original MIQP problem are formed. Since the solution of the QP problem is relatively simple, the suboptimal solution or global optimal solution of the MIQP problem which meets the integer constraints can be obtained by solving a series of QP problems.

The solution principle of the MIQP problem based on the Branch and Bound method can be further described by the binary search trees. Firstly, a vector $\alpha \in \{0, 1, *\}^{nd}$, whose dimension is identical with the decision variables $\boldsymbol{\gamma}_{\text{d}}$ which contains integer constraints, is defined. The vector $\boldsymbol{\varphi}$ not only corresponds to the nodes in the binary search trees, but also to the QP problems. For the MIQP problem, when the integer constraints in the decision variables γ_{d} are canceled, a new vector $\alpha_0 \in \{*, *, \ldots, *\}^{nd}$ can then be defined, in which the value is * means that this element can be defined as any real number between 0 and 1. Thus, the generation of the new QP problems can be achieved by selecting an element in $\boldsymbol{\varphi}_0$ which is defined as 0 and 1. For example, when the third element in α_0 is selected, the generation from parent node to two sub-nodes is shown in Fig. 10.

The resulting QP problems which correspond to the two new sub-nodes can be redefined as:

$$\min_{\gamma}(\gamma' H \gamma + F' \gamma) \tag{32a}$$

$$\text{subj.to.} \begin{cases} A_{\text{ineq}}\gamma \le b_{\text{ineq}} \\ A_{\text{eq}}\gamma = b_{\text{eq}} \\ \gamma \in \begin{bmatrix} \gamma_c \\ \gamma_d \end{bmatrix} \\ \gamma_c \in \Re^{nc} \\ \gamma_d(1) \in \Re \\ \gamma_d(2) \in \Re \\ \gamma_d(3) = 0 \\ \gamma_d(\#) \in \Re^{nd-3} \end{cases} \rightarrow \alpha_1 \quad \begin{cases} A_{ineq}\gamma \le b_{ineq} \\ A_{eq}\gamma = b_{eq} \\ \gamma \in \begin{bmatrix} \gamma_c \\ \gamma_d \end{bmatrix} \\ \gamma_c \in \Re^{nc} \\ \gamma_d(1) \in \Re \\ \gamma_d(2) \in \Re \\ \gamma_d(3) = 1 \\ \gamma_d(\#) \in \Re^{nd-3} \end{cases} \rightarrow \alpha_2 \tag{32b}$$

where H is the coefficient matrix with suitable dimensions,γ is the decision variables in the optimal control process for the MLD system, γ_c is the continuous decision variables, A_{ineq}, b_{ineq}, A_{eq} and b_{eq} are the coefficient matrices and vectors in the constrained inequalities and equalities. By solving the above two QP problems, the optimal decision variables are further sought [52,53]. If it is not successful, the other element in φ_0 will be set as 0 and 1; thus, the aforementioned solving process is repeated until the global optimal solution of the MIQP problem is generated.

9 Simulation results and analyses

In order to verify the performance of the proposed HMPC controller, which has been implemented using the Hybrid Toolbox [54], two simulation examples and the results are presented in this section. Note that since one of the major contributions of this study is to approximate the nonlinear tire longitudinal dynamics through the PWA approach, a more accurate system model, which also presents the best accuracy/simplicity compromise for control design use, is established in this paper. Therefore, to test the performance of the controller, we just intend to validate the longitudinal velocity tracking accuracy with slip occurrence. In addition, since most previous researches on vehicle velocity control are based on simple models not accounting for the tire–road interaction, the comparison between the performance of the proposed HMPC controller and the previous controllers cannot be achieved in this paper. The main simulation parameters are shown in Table 3.

To achieve the optimal control performance of the HMPC controller, the system control parameters need to be tuned first, which include the weighting parameters Q_y,$Q_{u1}$and Q_{u2}, and the control horizon N. Note that although the increment of the control horizon can improve the controller performance, the computation complexity will be increased dramatically, which is not conducive to the system's real-time control. Thus, the tuning objective of the control horizon is to make the N as small as possible, but, at the same time, the control performance should also be guaranteed. The optimization of other parameters is conducted through repeated simulation comparisons, and the parameters are determined finally for the optimal control performance. After the aforementioned tuning process, a satisfactory control performance is achieved with $N = 3$, $Q_{\text{y}} = 24$, $Q_{\text{u1}} = Q_{\text{u2}} = 8.5$.

Table 3 Simulation parameters of the intelligent vehicle

Parameter	Nominal value
m_{v} (kg)	2115
m_{c} (kg)	140
Θ (kgm^2)	5.65
r_{d}(m)	0.355
C_{D}	0.365
A(m^2)	3.26
ρ_{a} (kgm^{-3})	1.29
f_{R}	0.018

10 Simulation analysis of the first case

The first simulation condition is designed as a longitudinal velocity tracking with two different adhesion coefficients on a flat surface. The simulation results are shown in Figs. 11, 12, where A_s denotes the road adhesion coefficient. One can note that the designed controller follows the reference with minor errors in general for the two different road adhesion coefficients, except for the initial stages of the tracking procedure, in which the rising processes of the driving torque and the brake torque need some time.

It is also observed from Fig. 11 that during the velocity tracking procedure, the designed controller can calculate both the drive torque and the brake torque acted on the wheels that were needed, respectively, for the two different road adhesion coefficients. As shown in Fig. 12, for different road adhesion coefficients, to track the desired velocity, the drive torque and the brake torque acted on the wheels are also different, which is because the values of the tire longitudinal slip coefficients are controlled to be different during the velocity tracking procedure for different adhesion coefficients.

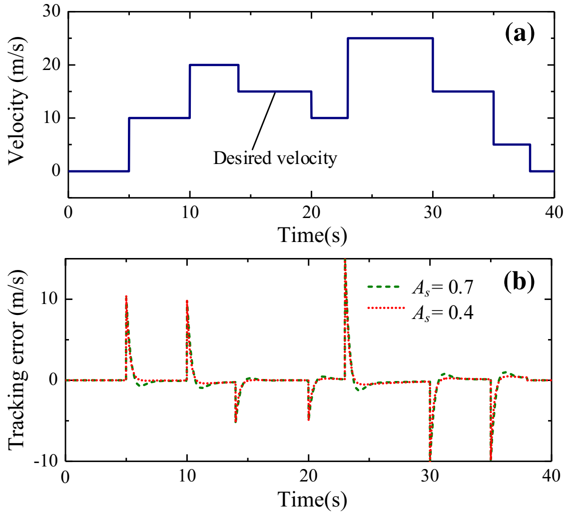

Fig. 11 Simulation results of the velocity tracking performance of the first case. **a** Desired velocity. **b** Velocity tracking error

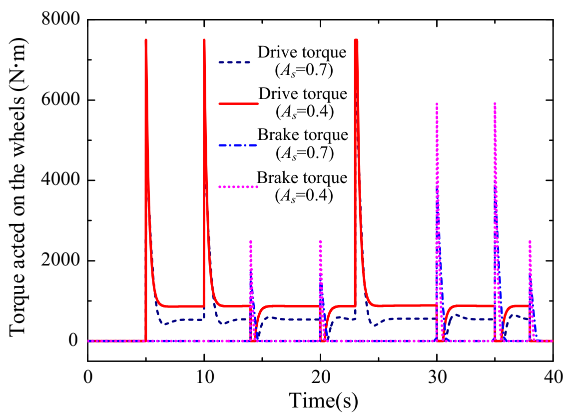

Fig. 12 The drive torque and the brake torque acted on the wheels for the first case

11 Simulation analysis of the second case

The second simulation test is performed when the reference velocity is set as a sinusoidal curve and the vehicle is assumed to be driven on a flat surface with two different adhesion coefficients. The simulation results are shown in Figs. 13, 14. As shown in Fig. 13, the controller is also able to react effectively to the sinusoidal variations of the vehicle longitudinal velocity. For both vehicle acceleration and deceleration, the velocity responses converge to the reference and present little tracking error for the two different adhesion coefficients. Figure 14 shows the drive torque and the brake torque acted on the wheels calculated by the designed

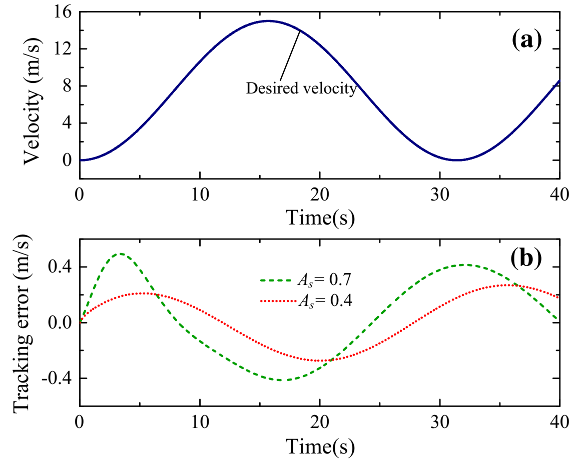

Fig. 13 Simulation results of the velocity tracking performance of the second case. **a** Desired velocity. **b** Velocity tracking error

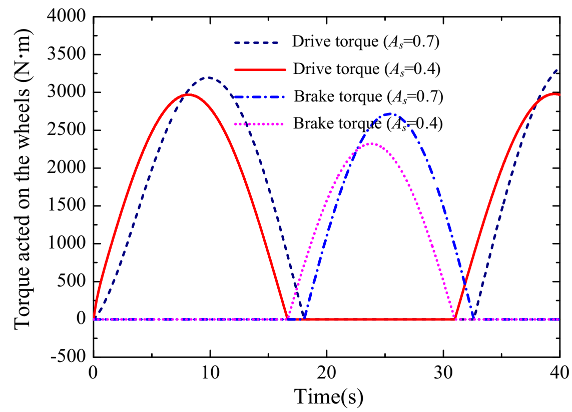

Fig. 14 The drive torque and the brake torque acted on the wheels for the second case

intelligent vehicle HMPC controller. It can be observed that the controller can effectively achieve different control actions for different road adhesion coefficients.

12 Simulation analysis of the third case

The third simulation test is performed when the reference velocity is set as the US06 cycle, which is a typical driving condition including high speed and high acceleration, with a fixed adhesion coefficient on a flat surface. The simulation results are shown in Figs. 15, 17. As shown in Fig. 15, the controller is able to react effectively to the variations of the vehicle longitudinal velocity. For both vehicle acceleration and deceleration, the velocity response converges to the refer-

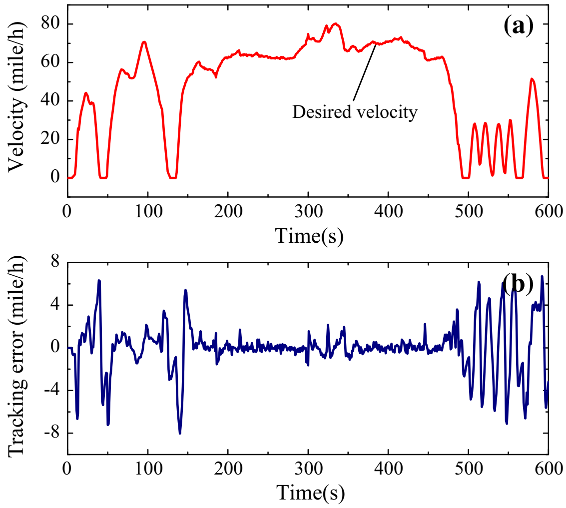

Fig. 15 Simulation results of the velocity tracking performance of the first case. **a** Desired velocity. **b** Velocity tracking error

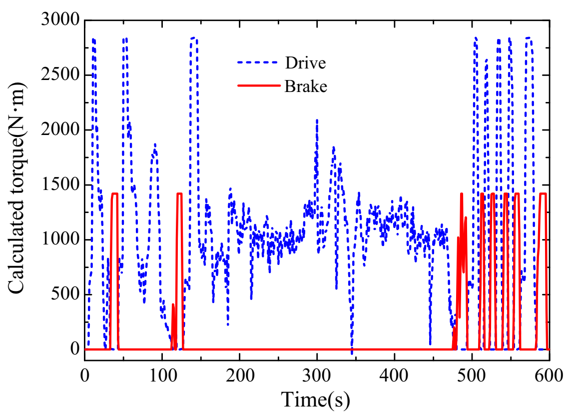

Fig. 16 Simulation results of the torques acted on the wheels

ence and presents little tracking error compared with the range of the desired values. The simulation results of the control signals during the US06 velocity tracking procedure are also shown in Figs. 16 and 17. It can be observed that the designed intelligent vehicle HMPC controller can calculate both the continuous torques acted on the wheels and the binary control outputs, i.e., the real-time statuses of δ_d and δ_b, which reflect the system operation modes, accurately. The mutual correspondence between the continuous and binary control variables is also verified by the simulation results, which demonstrates the correctness of the control logic.

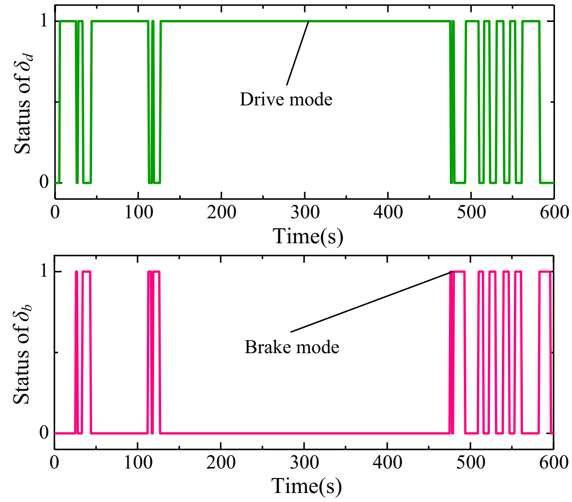

Fig. 17 Simulation results of the binary control signals

13 Conclusions

In this paper, to achieve the best model accuracy/simplicity compromise for the intelligent vehicle longitudinal velocity control design use, a novel PWA identification approach is proposed first to approximate the tire longitudinal dynamics. The system PWA identification problem is determined as constructing several affine submodels to approximate the nonlinear relationship between the tire longitudinal force and its influence factors. Comparisons between the PWA model output and the experimental data demonstrate the effectiveness of the proposed identification approach for the modeling of the tire longitudinal dynamics.

On this basis, considering the hybrid characteristics of the intelligent vehicle longitudinal dynamics with the PWA tire model, the system hybrid model is established based on the MLD framework, and the system HMPC control problem is then formulated as a MIQP problem, which is solved by the Branch and Bound method in this study. Two different simulation conditions are designed to verify the performance of the proposed HMPC controller, the simulation results show that the controller is able to react effectively to the variations of the vehicle velocity, and the velocity responses converge to the references well. The HMPC controller can not only provide the accurate torques acted on the wheels, which are the continuous control outputs, but also calculate the binary mode switching sequences.

In the future work of this paper, experimental validation of the effectiveness of the designed HMPC controller should be carried out. Note that since the HMPC optimal control problem needs to be solved over a finite horizon at each sampling time, which requires large computing power during implementation, the explicit form of the HMPC law can be computed offline by using multi-parametric programming technology (MPT) according to some of the latest studies.

Acknowledgements This work was supported by the National Natural Science Foundation of China (Grant Nos. 51705207, U1564201), the China Postdoctoral Science Foundation (Grant No. 2019T120401, 2017M611728), the Postdoctoral Research Foundation of Jiangsu Province (Grant No. 1701112B) and the Six Talent Peaks Project of Jiangsu Province (Grant No. GDZB-163).

Compliance with ethical standards

Conflict of interest The authors declare that they have no conflict of interest.

References

1. Jianguo, L., Sijian, L., Heng, F.: Analysis of AFS based on car navigation electronic map. J. Jiangsu Univ. Nat. Sci **39**(1), 1–6 (2018)
2. Sun, X., Cai, Y., Wang, S., et al.: Optimal control of intelligent vehicle longitudinal dynamics via hybrid model predictive control. Robot. Auton. Syst **112**, 190–200 (2019)
3. Li, Y., Zhang, B., Xu, X.: Robust control for permanent magnet in-wheel motor in electric vehicles using adaptive fuzzy neural network with inverse system decoupling. T. Can. Soc. Mech. Eng **42**(3), 286–297 (2018)
4. Ju, J., Haobin, J., Shidian, M.: Analysis on adaptive preview time of intelligent vehicle driver model. J. Jiangsu Univ. Nat. Sci **39**(3), 254–259 (2018)
5. Takase, M., Zhao, T., Zhang, M., et al.: An expatiate review of neem, jatropha, rubber and karanja as multipurpose non-edible biodiesel resources and comparison of their fuel, engine and emission properties. Renew. Sust. Energ. Rev **43**, 495–520 (2015)
6. Zhen, S., Shuo, L., Yantao, T., et al.: Intelligent vehicle's driver model considering longitudinal and lateral integrated control. In: ICMA, 5–8 August 2018, Changchun, China
7. Cerotti, D., Distefano, S., Merlino, G., et al.: A crowd-cooperative approach for intelligent transportation systems. IEEE Trans. Intell. Transp **18**(6), 1529–1539 (2017)
8. Daniel, A., Paul, A., Ahmad, A., et al.: Cooperative intelligence of vehicles for intelligent transportation systems (ITS). Wireless. Pers. Commun **87**(2), 461–484 (2016)
9. Yingfeng, C., Youguo, H., Hai, W., et al.: Pedestrian detection algorithm in traffic scene based on weakly supervised hierarchical deep model. Int. J. Adv. Robot. Syst **14**(1), 1–9 (2016)
10. Changzhu, Z., Jinfei, H., Jianbin, Q., et al.: A novel fuzzy observer-based steering control approach for path tracking in autonomous vehicles. IEEE Trans. Fuzzy. Syst **27**(2), 278–290 (2019)
11. Sun, X., Cai, Y., Wang, S., et al.: Piecewise affine identification of tire longitudinal properties for autonomous driving control based on data-driven. IEEE Access **6**, 47424–47432 (2018)
12. Xiaodong, S., Zhou, S., Long, C., et al.: Internal model control for a bearingless permanent magnet synchronous motor based on inverse system method. IEEE Trans. Energy Conver **31**(4), 1539–1548 (2016)
13. Omer, T., Unal, Y., Ahmet T.: Overview of battery charger topologies in plug-in electric and hybrid electric vehicles. In: ICCE, 9–11 May 2018, Famagusta, N. Cyprus
14. Thanok, S., Parnichkun, M.: Longitudinal control of an intelligent vehicle using particle swarm optimization based sliding mode control. Adv. Robotics **29**(8), 525–543 (2015)
15. Hong, L., Kil, T.C., Tae, S.N., et al.: Vehicle longitudinal brake control using variable parameter sliding control. Control. Eng. Pract **20**(1), 69–81 (2012)
16. Jullierme, D., Guilherme, P., Reinaldo, P.: Longitudinal model identification and velocity control of an autonomous car. IEEE Trans. Intell. Transp **16**(2), 776–786 (2015)
17. Lydie, N., Said, M.: Experimental vehicle longitudinal control using a second order sliding mode technique. Control. Eng. Pract **15**(8), 943–954 (2007)
18. Majdoub, K., Giri, F., Ouadi, H., et al.: Vehicle longitudinal motion modeling for nonlinear control. Control. Eng. Pract **20**(1), 69–81 (2012)
19. Dezao, H., Feng, G., Keqiang, L., et al.: Vehicle longitudinal dynamic model for vehicle collision avoidance systems. J. Tsinghua. Univ. Nat. Sci **44**(2), 258–261 (2004)
20. Konghui, G., Zhongcheng, Y., Dang, L.: A study on the prediction capability of UniTire model for combined slips mode. Auto. Eng **28**(6), 565–568 (2006)
21. Farroni, F., Lamberti, R., Mancinelli, N., et al.: TRIP-ID: A tool for a smart and interactive identification of Magic Formula tyre model parameters from experimental data acquired on track or test rig. Mech. Syst. Signal. Process **102**, 1–22 (2018)
22. Dugoff, P., Segel, L.: An analysis of tire traction properties and their influence on vehicle dynamic performance. SAE **3**, 1219–1243 (1970)
23. Pola, G., Benedetto, M.: Symbolic models and control of discrete-time piecewise affine systems: an approximate simulation approach. IEEE T. Automat. Contr **59**(1), 175–180 (2014)
24. Ding, Y., Zhu, C., Zhang, H.: A type of distribution control method for nonlinear stochastic systems. J. Drain. Irrig. Mach. Eng **35**(9), 774–779 (2017)
25. Arshad, M., Aly, R., Dianchen, L.: Bright-dark solitary wave solutions of generalized higher-order nonlinear Schrödinger equation and its applications in optics. J. Electromagnet. Wave **31**(16), 1711–1721 (2017)
26. Heemels, W., Schutter, B., Bemporad, A.: Equivalence of hybrid dynamical models. Automatica **37**(7), 1085–1091 (2001)
27. Xiaodong, S., Long, C., Haobin, J., et al.: High-performance control for a bearingless permanent magnet synchronous motor using neural network inverse scheme plus inter-

nal model controllers. IEEE Trans. Ind. Electron **63**(6), 3479–3488 (2016)

28. Wang, F., Xu, X., Fang, Z.: Design and analysis of herringbone gear with sixth-order transmission error based on meshing vibration optimization. Adv. Mech. Eng **9**(6), 1–12 (2017)
29. Li, Y., Zhang, B., Xu, X.: Decoupling control for permanent magnet in-wheel motor using internal model control based on back propagation neural network inverse system. B. Pol. Acad. Sci-Technol **66**(6), 961–972 (2018)
30. Georgios, P., Tobias, G., Manfred, M.: A hybrid model predictive control approach to the direct torque control problem of induction motors. Int. J. Robust. Nonlin **17**(17), 1572–1589 (2007)
31. Xu, L., Tseng, H., Hrovat, D.: Hybrid model predictive control of active suspension with travel limits and nonlinear tire contact force. In: ACC, July 2016, Boston, USA
32. Eduardo, P., Aldo, C.: Hybrid model predictive control for flotation plants. Miner. Eng **70**, 26–35 (2015)
33. Xiaoqiang, S., Yingfeng, C., Chaochun, Y., et al.: Vehicle height and leveling control of electronically controlled air suspension using mixed logical dynamical approach. Sci. China. Technol. Sci **59**(12), 1814–1824 (2016)
34. Sun, X., Cai, Y., Yuan, C., et al.: Hybrid model predictive control of damping multi-mode switching damper for vehicle suspensions. J. Vibroeng **19**(4), 2910–2930 (2017)
35. Wang, G., Yin, M., Liang, C.: Measurement system of tire footprint geometric parameters based on image processing. J. Jiangsu Univ. Nat. Sci **38**(2), 139–143 (2017)
36. Ma, B., Lv, C., Liu, Y., et al.: Estimation of road adhesion coefficient based on tire aligning torque distribution. J. Dyn. Syst-T. ASME **140**(5), 1–17 (2018)
37. Roll, J., Bemporad, A., Ljunge, L.: Identification of piecewise affine system via mixed-integer programming. Automatica **40**(1), 37–50 (2004)
38. Vaezi, M., Izadian, A.: Piecewise affine system identification of a hydraulic wind power transfer system. IEEE T. Contr. Syst. T **23**(6), 2077–2086 (2015)
39. Paoletti, S.: Identification of piecewise affine models, Ph.D. dissertation, University of Siena, Siena, Italy (2004)
40. Xu, X., Chen, T., Chen, L., et al.: Longitudinal force estimation for motorized wheels driving electric vehicle based on improved closed-loop subspace identification. J. Jiangsu Univ. Nat. Sci **37**(6), 650–656 (2016)
41. Wang, F., Xu, X., Fang, Z.: Study of the influence mechanism of pitch deviation on cylindrical helical gear meshing stiffness and vibration noise Adv. Mech. Eng **9**(9), 1–9 (2017)
42. Murat, Y., Philip, T.K.: Review of battery charger topologies, charging power levels, and infrastructure for plug-in electric and hybrid vehicles. IEEE Trans. Power. Electr **28**(5), 2151–2169 (2013)
43. Keiya, N., Jingyu, Z., Xianyin, L., et al.: Effects of micro-hole nozzle and ultra-high injection pressure on air entrainment, liquid penetration, flame lift-off and soot formation of diesel spray flame. Int. J Engine. Res **18**(1–2), 51–65 (2017)
44. Guo, J., Dong, H., Sheng, W., et al.: Optimum control strategy of regenerative braking energy for electric vehicle. J. Jiangsu Univ. Nat. Sci **39**(2), 132–138 (2018)
45. Sun, X., Cai, Y., Chen, L., et al.: Vehicle height and posture control of electronic air suspension system using hybrid system approach. Veh. Syst. Dyn **54**(3), 328–352 (2016)
46. Zhang, Y., Wei, Z., Zhu, X., et al.: Control strategy for precision water-fertilizer irrigation system and its verification. J. Drain. Irrig. Mach. Eng **35**(12), 1088–1095 (2017)
47. Pregelj, B., Gerksic, S.: Hybrid explicit model predictive control of a nonlinear process approximated with a piecewise affine model. J. Process. Control **20**(7), 832–839 (2010)
48. Torrisi, F., Bemporad, A.: HYSDEL-A tool for generating computational hybrid models for analysis and synthesis problems. IEEE Trans. Control Syst. Technol **12**(2), 235–249 (2004)
49. Hredzak, B., Agelidis, V., Demetriades, G.: Application of explicit model predictive control to a hybrid battery-ultracapacitor power source. J. Power. Sources **277**, 84–94 (2015)
50. Xiaodong, S., Long, C., Zebin, Y., et al.: Speed-sensorless vector control of a bearingless induction motor with artificial neural network inverse speed observer. IEEE/ASME Trans. Mech **18**(4), 1357–1366 (2013)
51. Owusu, E., Zhan, Y., Mao, Q.: An SVM-AdaBoost facial expression recognition system. Appl. Intell **40**(3), 536–545 (2014)
52. Sun, X., Cai, Y., Yuan, C., et al.: Fuzzy sliding mode control for the vehicle height and leveling adjustment system of an electronic air suspension. Chin. J. Mech. Eng **31**(25), 1–13 (2018)
53. Wang, F., Xu, X., Fang, Z.: New method with experimental validation for power transmission process analysis on herringbone gear train system Int. J. Acoust. Vib **22**(4), 519–535 (2017)
54. Geyer, T., Papafotiou, G., Morari, M.: Hybrid model predictive control of the step-down DC-DC converter. IEEE Trans. Control Syst. Technol **16**(6), 1112–1124 (2008)

Publisher's Note Springer Nature remains neutral with regard to jurisdictional claims in published maps and institutional affiliations.